Wear 350-351 (2016) 1–9

Contents lists available at ScienceDirect

Wear

journal homepage: www.elsevier.com/locate/wear

Low humidity-sensitivity of MoS_2/Pb nanocomposite coatings

Hao Li [a,c], Guangan Zhang [a,*], Liping Wang [a,b,**]

[a] State Key Laboratory of Solid Lubrication, Lanzhou Institute of Chemical Physics, Chinese Academy of Sciences, Lanzhou 730000, China
[b] Key Laboratory of Marine Materials and Related Technologies, Zhejiang Key Laboratory of Marine Materials and Protective Technologies, Ningbo Institute of Materials Technology and Engineering, Chinese Academy of Sciences, Ningbo 315201, China
[c] University of Chinese Academy of Sciences, Beijing 100049, China

ARTICLE INFO

Article history:
Received 31 July 2015
Received in revised form
15 December 2015
Accepted 22 December 2015
Available online 30 December 2015

Keywords:
Sliding wear
Sliding friction
Solid lubricant coatings
Tribophysics
Tribochemistry

ABSTRACT

Optimizing the MoS_2-based coating to overcome its humidity sensitivity is still a challenge. In this work, MoS_2/Pb composite coatings with various Pb contents were synthesized by unbalanced magnetron sputtering system. The microstructures of the coatings change from loose columnar structure for pure MoS_2 to a compact featureless structure for Pb doped MoS_2. The hardness and elastic modulus of the MoS_2/Pb composite coatings gradually increase with the Pb content increase and exhibit a maximum value at Pb content of 8.9 at%. Further increase in the Pb content results in a decrease in the hardness and elastic modulus of the coatings. The tribological performance of the coatings was systematically evaluated under different humidity conditions, and the underlying mechanisms were investigated. The results show that the mechanical property of the coating determines the wear properties under dry air; whereas the antioxidant property of the coating becomes prominent with regard to the wear-resistant in humid environmental. This benefits us to tailor or select the MoS_2-based composite coatings for different operating conditions.

1. Introduction

Solid lubricant coatings based on transition metal dichalcogenides (TMDs) constitute a group of promising candidates for many applications, such as high vacuum, aerospace, high-speeds, high loads, where liquid lubrication is not available [1]. The excellent tribological properties of TMDs are thought to be associated with “easy shear” planes in the ⟨0001⟩ crystallographic direction [2], resulting in very low shear strength as low as dozens of MPa [3]. The “easy shear” properties of TMDs can be explained by the dz^2 character of the highest occupied molecular orbital (HOMO) [4]. More precisely, in MoS_2, the dz^2 orbital is filled, leaving only high energy antibonding orbitals available for interlayer bonding; therefore, the interaction between the interlayer is weak, which results in very low shear strength. MoS_2, as the most abundant TMD (termed molybdenite), has been extensively studied compared to the other TMDs, such as WS_2, WSe_2 and $MoSe_2$. However, MoS_2 is very sensitive to moisture; the dangling and unsaturated bonds of the crystal MoS_2 are easy attracted by H_2O to MoO_3 and H_2S (gaseous), which causes a higher friction coefficient because of increasing shear strength of MoO_3 [4,5]. The disadvantage of MoS_2 restricts the technological applications in the Earth's atmosphere. However, there is increasing demand for environmentally robust solid lubricant coatings that can adapt themselves to different environments. For instance, aircrafts are repeatedly subjected to high and low humidity with altitude changes. Satellites have to be exposed to moisture during assembly or launch, and attacked by atomic oxygen in low Earth orbit. For this reason, optimizing the MoS_2 coating becomes an important way to meet the challenges. Changing crystallographic orientation of MoS_2 from *Random-oriented* to *basal-oriented* is an effective way to improve the wear behavior of MoS_2 coatings in humid air, as the ratio of the oxidation rate along the *c*-axis to the one parallel to the basal plane is 10^{-11} at ideal perfect sites on the basal surface [6,7]. Further, Chhowalla et al. [8] improved the tribological and antioxidant properties of MoS_2 by using MoS_2 in the form of isolated inorganic fullerene-like hollow nanoparticles. However, it is hard to succeed in the applications of the novel MoS_2 coating as the requirement of the special equipment and complex deposition processes. Otherwise, doping with another element or compound in the MoS_2 coating is an economical and effective way to improve its tribological properties, the dopants include metals [9,10–16], nonmetals [17–19], and compounds [20–23]. Different doping elements play different roles in modifying the wear behavior of MoS_2. Teer et al. [24] suggested that Ti

* Corresponding author.
** Corresponding author at: State Key Laboratory of Solid Lubrication, Lanzhou Institute of Chemical Physics, Chinese Academy of Sciences, Lanzhou 730000, China. Tel.: +86 931 4968080; fax: +86 931 4968163.
E-mail addresses: gazhang@licp.cas.cn (G. Zhang), lpwang@licp.cas.cn (L. Wang).

http://dx.doi.org/10.1016/j.wear.2015.12.008
0043-1648/

atoms were situated between the neighboring S planes, which is responsible for reducing the sensitivity of the coating to water vapor. The oxygen substituted for sulfur within the lattice of MoS_2 could help reduce the friction [19]. Isaeva et al. [25] reported that 21–24% of the N atoms in amorphous W–S–N coating form quasi-free N_2 molecules, such N_2 units were located in cages in the amorphous matrix, where they were coordinated mainly by S atoms. This structure made it easy access to W and S for continuous formation of WS_2 in the contact region, and resulted in ultra-low friction for an amorphous W–S–N film [26]. Voevodin et al. found [27] that the WC/DLC/WS_2 composite coating exhibited excellent friction recovery in humid-dry environmental cycling. The DLC phase is responsible for lubrication in humid environments while the WS_2 phase is contributed to lubrication in dry nitrogen and vacuum. Zabinski et al. [28] found the Sb_2O_3 particles inside the $MoS_2/Sb_2O_3/C$ composite coating could effectively block the propagation of cracks perpendicular to the substrate, and hence slowed the coating delamination/wear-off. However, for the most doped elements and compounds, which neither interact with MoS_2 nor play special role in improving the wear behavior of MoS_2. Those dopants can modify the coating microstructure, adjust the residual stress state in the coating and the hardness-to-modulus ratio, and then improve wear resistance under humidity conditions [29].

Among the doped elements, Pb is one of the most promising candidates for dopants, as Pb itself is an excellent solid lubricant [30], and Pb can prevent the formation of randomly oriented MoS_2 in the sputtering plasma [31]. Thus, MoS_2/Pb composite coatings exhibit superior wear resistance [32]. However, it is rarely reported the effect of the Pb content on the friction coefficient and wear rate of the MoS_2/Pb composite coatings under various environment. Moreover, the friction and wear mechanism of MoS_2/Pb composite coatings under different humidity conditions is still unclear. In this study, the MoS_2/Pb composite coatings were deposited using unbalanced magnetron sputtering system. The effects of the Pb content on the wear behavior of the MoS_2/Pb composite under three different environments were investigated, and the main factors that influenced the wear properties of MoS_2/Pb composite coatings under different humid conditions were discussed systematically.

2. Experimental details

MoS_2/Pb composite coatings were deposited on 304 stainless steel and silicon wafer using a Teer UDP-650 unbalanced magnetron sputtering system. The sputtering system contains two MoS_2 targets, one titanium target and one Pb target, and the substrates rotate among the targets, the schematic diagram of the deposition system is shown in Fig. 1. Before deposition, the vacuum chamber was evacuated to a background vacuum of 1.33×10^{-3} Pa using a diffusion pump backed by a rotary pump, and then the substrates were etched by Ar^+ ion for 30 min with a DC bias of -500 V. Afterwards, all the four targets were sputter-cleaned for 5 min. Prior to the deposition of composite coatings, a Ti interlayer of approximately 200 nm thickness was deposited on the substrates to improve the adhesion properties and load bearing capacity, followed a gradient interlayer. The gradient interlayer was deposited by sputtering from four targets simultaneously, with the power on the titanium target being gradually reduced while the power on the MoS_2 targets and Pb target increased. A DC substrate bias of -50 V was applied during the deposition. For all the experiments, the target current for the MoS_2 targets was fixed at 0.8 A while the sputtering current applied on the Pb target was adjusted from 0 to 0.4 A.

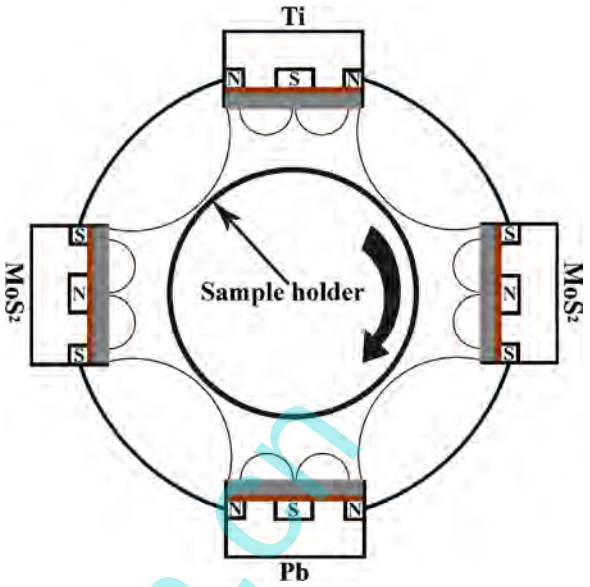

Fig. 1. Schematic diagram of the deposition system.

The surface and cross-sectional micrographs of the MoS_2/Pb composite coatings were performed by field emission scanning electron microscopy (FESEM, Hitachis-4800). Atomic force microscopy (AFM, Benyuan CSPM 4000) under contact mode was used to measure the surface roughness of the MoS_2/Pb composite coatings. The compositions of the coatings were analyzed by energy-dispersive X-ray spectroscopy (EDS, Oxford Inca Energy 250) and X-ray photoelectron spectroscopy (XPS, PHI-5720) with Al Kα radiation. Philips X'perts X-ray diffractometer with Cu Kα radiation was used to measure the structures of the coatings. The hardness of the as-deposited coatings was investigated by a nano-indenter (MTS NanoIndenter G200), a Berkovich diamond tip was used and continuous stiffness option was adopted, the maximum indentation depth was 200 nm (less than 10% of total coating thickness to minimize the substrate contribution). Six replicate indentations were made for each coating sample and the hardness was calculated from the load–unloading curves.

The tribological performances under ambient pressure were evaluated using a ball-on-disk reciprocating sliding tribometer (CSM, Tribo-S-D-0000) at room temperature. The humidity was fixed at $13 \pm 1.5\%$, $35 \pm 3\%$, and $75 \pm 3\%$ RH respectively. As one of the most commonly used high-chromium bearing steels, GCr15 was used as sliding mating materials. The diameter of the tribo-pair was 4 mm, and the fiction tests were conducted under a constant load of 5 N; therefore, the Hertzian contact pressures were between 874.2 and 1034 MPa correspondingly, and this was in the high contact stress regime that MoS_2-based coatings were usually used [10]. The reciprocating amplitude was 5 mm, the frequency was 5 Hz, and the total reciprocating cycle number was 10,000 cycles. In addition, environmental adaptability of the coatings were investigated by switching environment between dry air ($13 \pm 1.5\%$ RH) and humid air ($75 \pm 3\%$ RH) every 5000 cycles, for total test duration of 30,000 cycles. For this investigation, dry air was obtained from refrigerated air dryer, the humid air was obtained by a humidifier; the humidity was precise controlled by mixing dry air and humid air in a proper ratio. The contact mating surfaces were investigated by Micro-Raman spectrometer (Jobin Yvon LabRAM HR800 UV, YGA 532 nm). The wear scars on the tribo-pairs were characterized by JSM-5600 SEM. The wear rates (K) of coatings were calculated via $K=V/(FS)$, where V was the wear volume loss in mm^3, F was the applied normal load in Newton and S was the sliding distance in meters, and the wear

Table 1
Deposition parameters, element content and surface roughness of the MoS_2/Pb composite coatings.

Run no.	Target current (A)		Mo (at%)	S (at%)	Pb (at%)	O (at%)	Ra (nm)
	MoS_2	Pb					
1	0.8	0	33.8	54.6	0	11.6	4.32
2	0.8	0.1	36.5	53.7	2.3	7.5	3.42
3	0.8	0.15	36.1	53.9	4.1	5.9	2.48
4	0.8	0.2	33.9	54.2	6.8	5.1	1.67
5	0.8	0.25	33.7	54.8	7.6	3.9	1.17
6	0.8	0.3	33.7	53.2	8.9	4.2	1.15
7	0.8	0.35	30.6	54.4	10.4	4.6	1.10
8	0.8	0.4	50.6	50.2	14.8	4.4	1.00

volumes of the coatings were obtained via equation $V=l\times S$, where l was the amplitude of the wear track, S was the wear track depth profiles measured by an Alpha-Step D-100 profilometer.

3. Results and discussion

3.1. Composition and microstructure

The compositions for pure MoS_2 and MoS_2/Pb composite coatings were analyzed by EDS, as shown in Table 1, the element compositions of Mo, S, Pb and O were normalized to 100 at%. The Pb content varies from 0 to 14.8 at% as Pb target current increases. It is seen that the O content decreases with increasing the Pb content.

The XRD patterns of pure MoS_2 and MoS_2/Pb composite coatings are shown in Fig. 2. There is a remarkable peak at around $2\theta=13°$ for pure MoS_2 coating, which is assigned to the MoS_2 (002) plane, the peaks at around $2\theta=33°$ and 59° are ascribe to the MoS_2 (100) and (110) planes respectively [33,34]. This results indicate that pure MoS_2 with its basal planes mainly oriented parallel to the substrate, and this oriented coating shows high oxidation resistance and long wear life [35]. However, the MoS_2 (100) and (110) peaks disappear when Pb is incorporated into the MoS_2 coating. The presence of Pb during deposition leads to re-arrangement of the deposited MoS_2 and the formation of the nucleation sites favoring basal crystalline growth [31]. Moreover, as the Pb content increases, the appearance of a broad bump is accompanied by the decreasing of (002) peak, which implies that the coatings are amorphous. Therefore, the growth of the MoS_2 crystalline is restricted by the Pb doping. The cross-section and surface morphologies of the pure MoS_2 and MoS_2/Pb composite coatings are illustrated in Fig. 3. The MoS_2 coating reveals a typical porous with column morphology as shown in Fig. 3a, while the MoS_2/Pb composite coatings show a dense and featureless morphology even when the Pb content as low as 2.3 at%. Furthermore, as shown in Table 1, the Roughness average (Ra) of the coatings decreases as the Pb content increases, which also confirms that the composite coatings with high Pb content exhibit dense morphology.

The XPS spectra of pure MoS_2 and MoS_2 doped with 6.8 at% Pb composite coatings are shown in Fig. 4. The surface of the coating was firstly analyzed by XPS, then, the subsurface layer was etched by Ar^+ ion for 20 s for further analysis. The etching was carried out to check the antioxidant capability of the MoS_2/Pb composite coating after 15 days of store in ambient air (50% RH) and ensure that the tested material represented the bulk coating. The Mo 3d3/2 peak at binding energy position of 231.4 eV corresponds to Mo^{4+} ions like those present in MoS_2, while the Mo 3d3/2 peak at 235.0 eV is assigned to Mo^{6+} in MoO_3 [36]. The Pb 4f 7/2 peak at binding energies of 137.4 eV is between the position of Pb and PbO_x [37] or PbS [38,39], indicating that partial of the Pb in the coating is in the oxygen or sulfur environment. However, it is

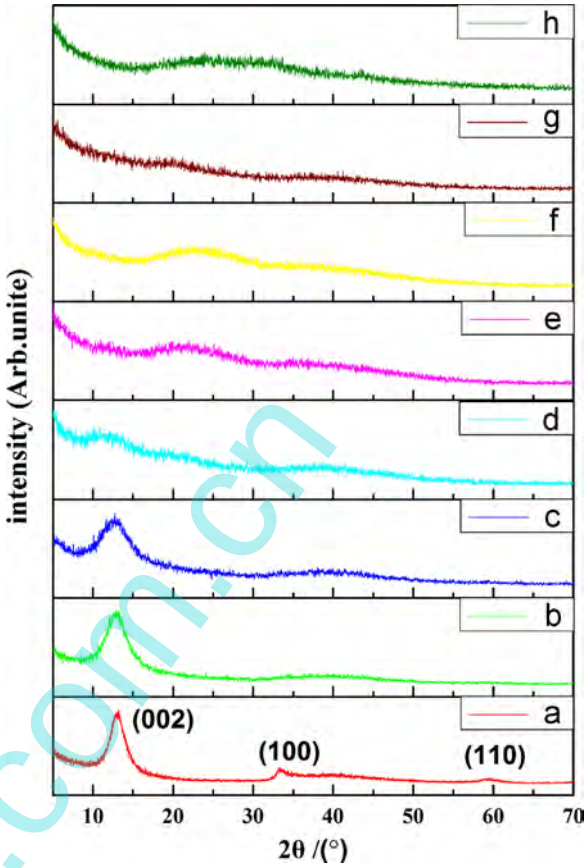

Fig. 2. XRD patterns of (a) MoS_2, and MoS_2/Pb composite coatings at Pb contents of (b) 2.3 at%, (c) 4.1 at%, (d) 6.8 at%, (e) 7.6 at%, (f) 8.9 at%, (g) 10.4 at% and (h) 14.8 at%.

difficult to distinguish the chemical state of element Pb due to the similar binding energies between PbS and PbO_x. The S 2p3/2 peak at binding energies of 161.6 eV is assigned to MoS_2 [40,41]. The O 1s peak at binding energies of 532.1 eV is ascribed to absorbed oxygen (molecular oxygen) [42]. After Ar^+ ion etching for 20 s, MoO_3 was hardly detected. The binding energy of Mo 3d drops to a lower level, which suggests that Mo in the bulk of the coating is less influenced by oxygen. The Pb 4f 7/2 peak at binding energies of 136.9 eV is on the position of Pb [43]. No obvious peak shift is found for S 2p3/2. However, a weak O 1s peak is still observed at the position of the O–Mo bond (529.8 eV [43]). The result shows that the MoS_2/Pb composite coating is mainly composed of MoS_2 and metallic Pb, and part of MoS_2 is oxidized during deposition; there is no interaction between Pb and MoS_2.

3.2. Mechanical properties

The hardness and elastic modulus of the MoS_2 and MoS_2/Pb composite coatings were measured and the results are given in Fig. 5a. As the Pb content increases from 2.3 to 8.9 at%, the hardness of the composite coatings increases from 4.6 to 7.2 GPa significantly, which is higher than that of pure MoS_2 coating (around 4.3 GPa). The lower hardness of the pure MoS_2 coating is related to its columnar morphologies and porous structure. The hardness enhancement of the composite coatings is ascribed to the densification of the coatings. However, the hardness of the composite coatings decreases from 7.2 to 3.8 GPa with further increasing of the Pb content from 8.9 to 14.8 at%. A similar behavior of metals doped MoS_2 coatings had been reported in MoS_2–Cr and MoS_2–Ti composite coating [44]. There are two reasons for the reduction of hardness with increasing of metal dopant: one is the negative

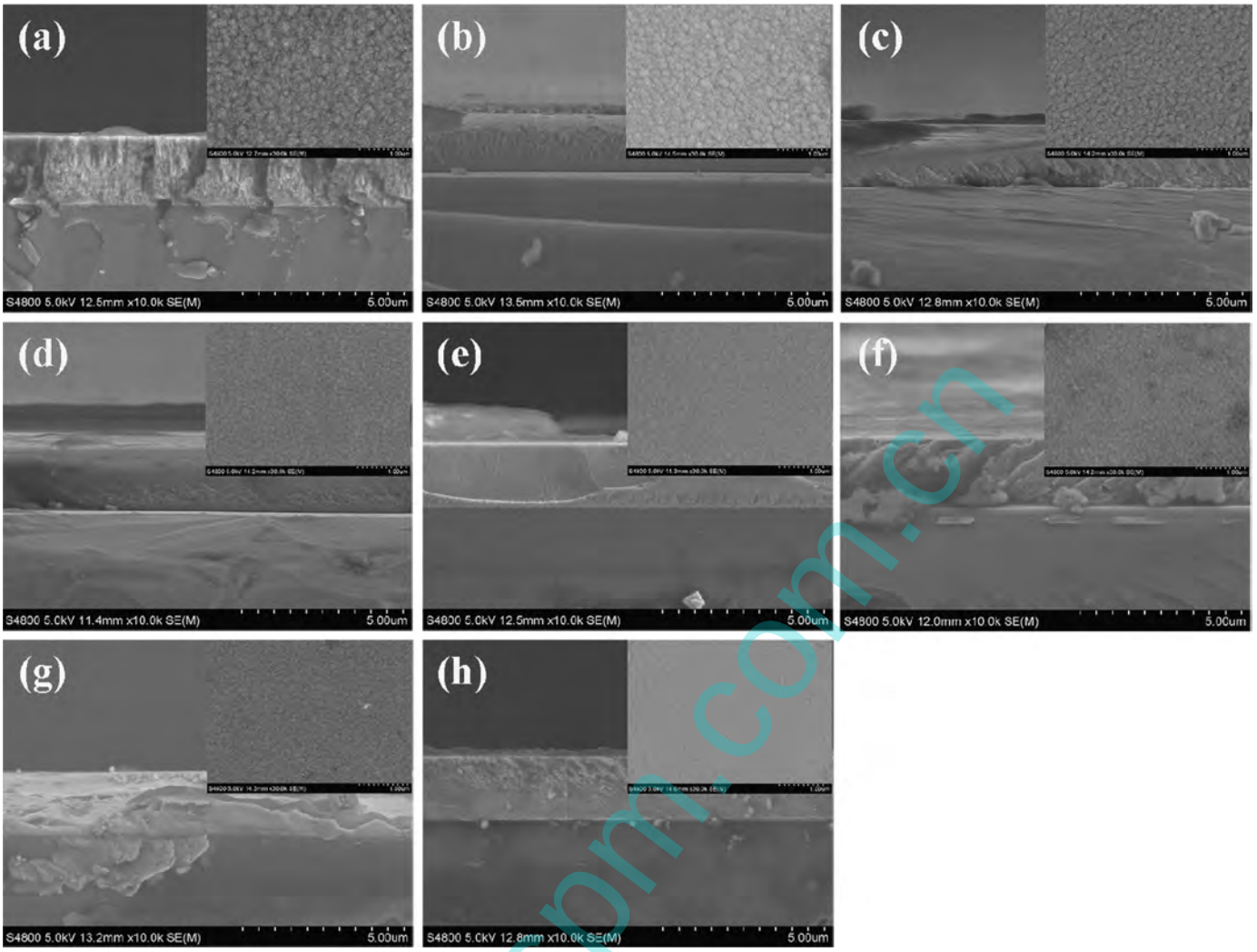

Fig. 3. FESEM micrographs of (a) MoS_2, and MoS_2/Pb composite coatings at Pb contents of (b) 2.3 at%, (c) 4.1 at%, (d) 6.8 at%, (e) 7.6 at%, (f) 8.9 at%, (g) 10.3 at% and (h) 14.8 at%.

Hall–Petch dependence of the hardness on the grain size, and the other is the deformation of soft metal grains. According to the Hall–Petch relationship, the hardness of the MoS_2/Pb composite coatings increases with the decreasing crystallite size as the discussion in the XRD and SEM results. However, when the crystallite size decreases below a certain limit or the coating appears amorphous structure, the fraction of grain boundaries increases rapidly and the strength and hardness of the coatings decreases due to a grain boundary sliding [45–47]. Otherwise, Pb forms separate grains when the Pb content is high enough in the MoS_2/Pb composite coatings. The Pb grains in the composite coatings relax the compressive stress, and Pb is easy to deform under external penetration, which results in the decrease of the hardness [48].

The same trend is seen in elastic modulus. With the Pb content increasing from 0 to 8.9 at%, the elastic modulus of the composite coatings increases from 68.8 GPa for pure MoS_2 to 92.3 GPa. For a further increase of the Pb content up to 14.8 at%, the elastic modulus decreases from 92.3 GPa to 65.5 GPa. For an excellent performance of coatings in mechanical and tribological testing not only high hardness (H) but also a low elastic modulus (E) is favorable. The ratio of the hardness to the elastic modulus H/E, which is also called the plasticity index, is often a reliable indicator of wear resistance for a coating [49]. Therefore, the wear resistance of a coating could be improved for a high H/E value. Fig. 5b shows the H/E values varied as the function of the Pb content for the as-prepared MoS_2/Pb composite coatings. In lower metal content region, the H/E values increase with the increasing of doping content. A maximum H/E value of about 0.078 is obtained at around 8.9 at% Pb for the composite coatings. Then the H/E values decrease rapidly with further increasing of the Pb content.

3.3. Tribological behavior under different humidity conditions

To investigate the effect of the Pb content on the friction and wear behaviors of the MoS_2-based coatings, the tribological behavior of the as-fabricated coatings was performed under various ambient air environments including 13%, 35%, and 75% RH. Fig. 6 shows the average friction coefficient and wear rate of the MoS_2 and MoS_2/Pb composite coatings against GCr15 under three different humidity conditions. The results show that the wear rates of MoS_2/Pb composite coatings are lower than pure MoS_2 under three different humidity conditions, and for all the coatings, the average friction coefficients and wear rates increase with increasing humidity levels. The significant differences between friction in dry and humid air indicate a detrimental influence of the humidity, whereas the effect of oxygen is minimal.

As shown in Fig. 6a, the friction coefficients obtained from both MoS_2 and MoS_2/Pb composite coatings are close to each other under dry air (13% RH). In other words, the antioxidant property of the MoS_2/Pb composite coatings shows little effect on the friction

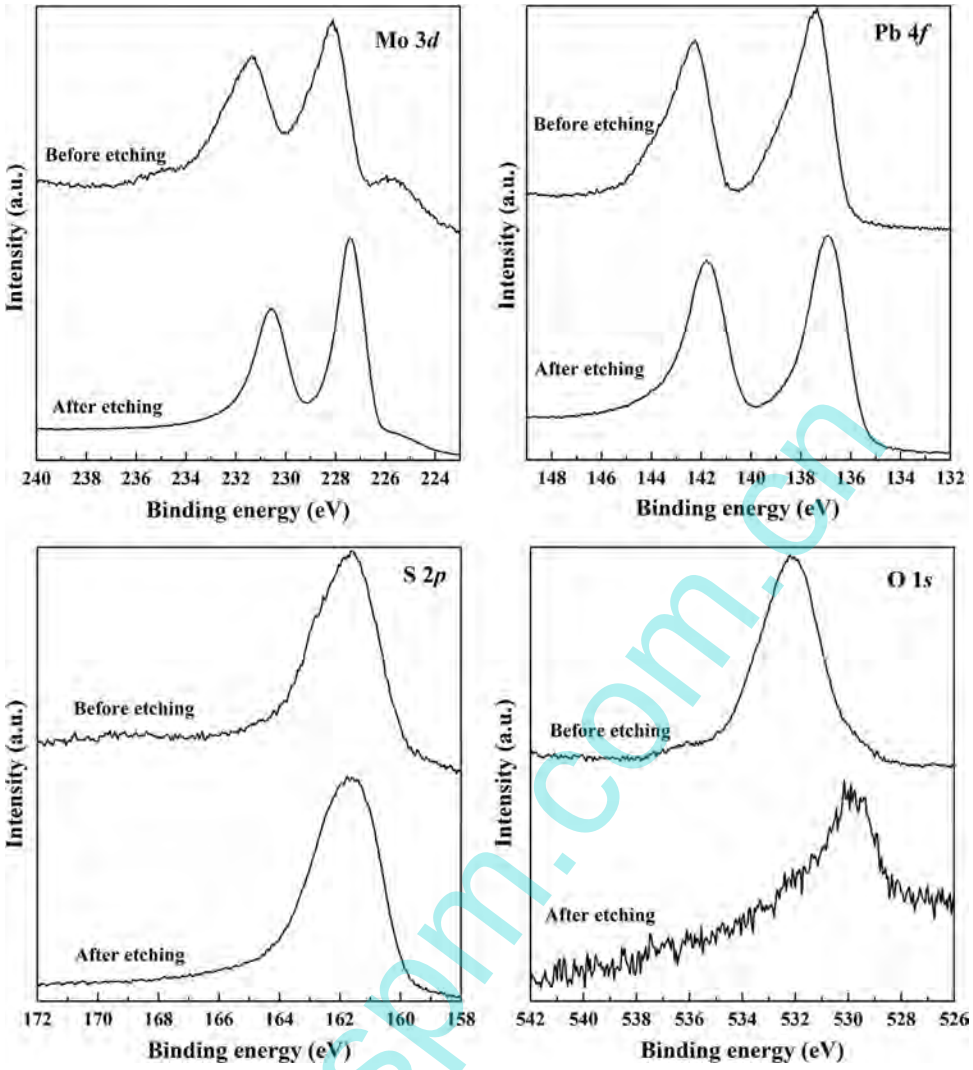

Fig. 4. XPS spectra of Mo 3d, Pd 4f, S 2p and O 1s measured before and after Ar etching.

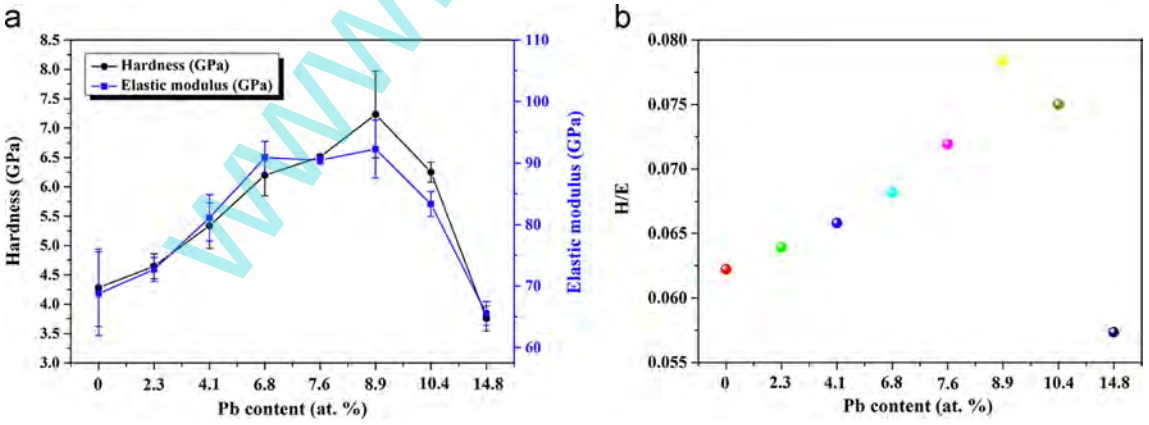

Fig. 5. (a) Hardness and elastic modulus of MoS_2 and MoS_2/Pb composite coatings. (b) H/E values of MoS_2 and MoS_2/Pb composite coatings.

coefficient. However, the wear rates of the composite coatings decrease from 5.07×10^{-7} mm^3/Nm for pure MoS_2 coating to 1.47×10^{-7} mm^3/Nm for the MoS_2-8.9 at% Pb composite coating and then increase dramatically with further increasing the Pb content. All the MoS_2/Pb composite coatings show better wear resistance than pure MoS_2. The H/E values in Fig. 5 show a good relation and tendency with the wear rate in 13% RH (Fig. 6a), except for pure MoS_2. However, the MoS_2-14.8 at% Pb composite coating still exhibits a lower wear rate than that of pure MoS_2, though the pure MoS_2 even with a lower H/E value. It is supposed that MoS_2 oxidize easily even under 13% RH condition. Fig. 7 shows the XPS spectra of wear tracks for pure MoS_2 and the MoS_2-14.8 at% Pb composite coatings tested in

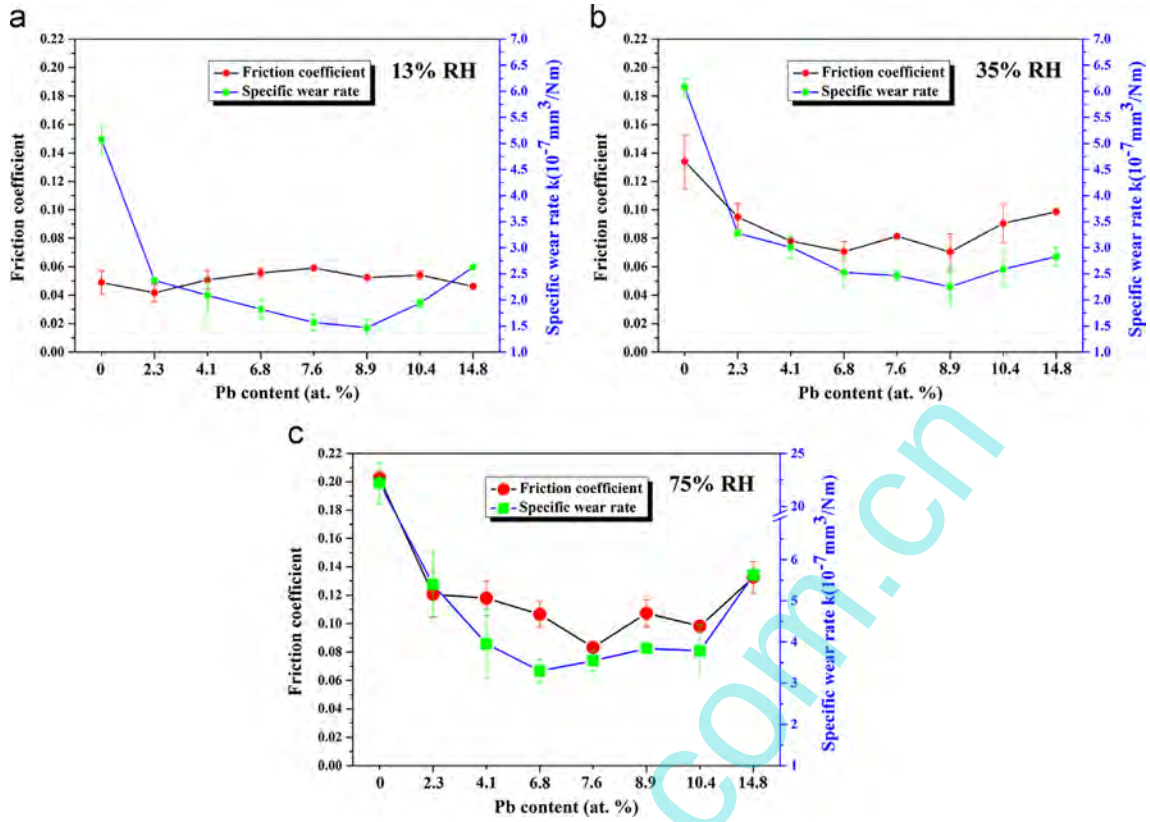

Fig. 6. Average friction coefficient and wear rate of MoS_2 and MoS_2/Pb composite coatings at (a) 13%, (b) 35% and (c) 75% RH.

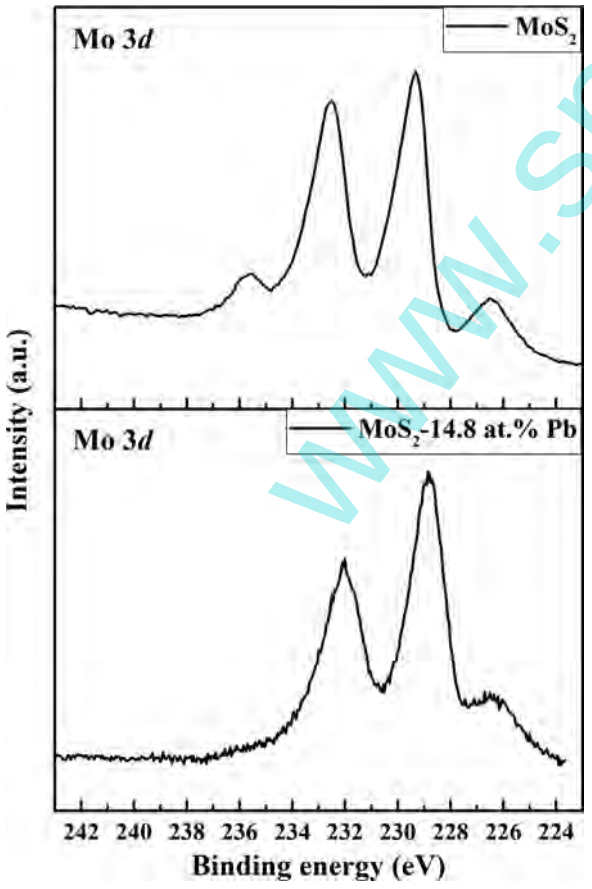

Fig. 7. XPS spectra of wear tracks for pure MoS_2 and MoS_2-14.8 at% Pb composite coatings tested in 13% RH.

13% RH. For pure MoS_2 coating, the Mo 3d3/2 peak at 235.0 eV is assigned to Mo^{6+} in MoO_3 [36], while no signal of Mo oxidation products is detected for the MoS_2-14.8 at% Pb composite coating. It is obviously that the MoS_2/Pb coatings show better antioxidant property, and their wear rates are less influenced by oxidation. Therefore, the tribological performance of the MoS_2/Pb composite coatings under dry air is mainly determined by the mechanical properties. Similar to Au, Ti and Cr doped MoS_2 coatings [50], the average friction coefficients and wear rates of the composites coatings are generally lower than that obtained for the pure MoS_2 in 35% RH, which is attributed to a relatively denser structure [9]. The friction coefficient decreases from 0.13 for pure MoS_2 coating to a minimum level around 0.070 for the MoS_2-8.9 at% Pb composite coating, and then increases to 0.099 with further increasing Pb content to 14.8 at%. The wear rate under 35% RH remains consistent with the changes under 13% RH condition. It is clear that the antioxidant properties of the MoS_2/Pb composite coatings become prominent as the humidity level increases, but the mechanical properties of the coatings still play a vital role in determine the wear rate. Under humid condition (75% RH), relatively low levels of dopant (2.3 at%) leads to a significant decrease in friction coefficient and wear rate. The friction coefficient of the coatings decreases rapidly to minimum value of approximately 0.083 for the MoS_2-7.6 at% Pb composite coating. However, further increase of the Pb content results in an increase of the friction coefficient. Although the wear rate shows the same trend as that in 35% RH, the minimum wear rate is obtained by the MoS_2-6.8 at% Pb composite coating. It is obviously that the tribological behavior of the composited coatings under humid condition (75% RH) is not determined by the mechanical properties, as the friction coefficient and wear rate is no longer in accord with the H/E values. There was no significant association between wear, friction coefficient and density of the coatings, which suggests that the tribological behavior under humid air is not influenced by the density of the composite coatings.

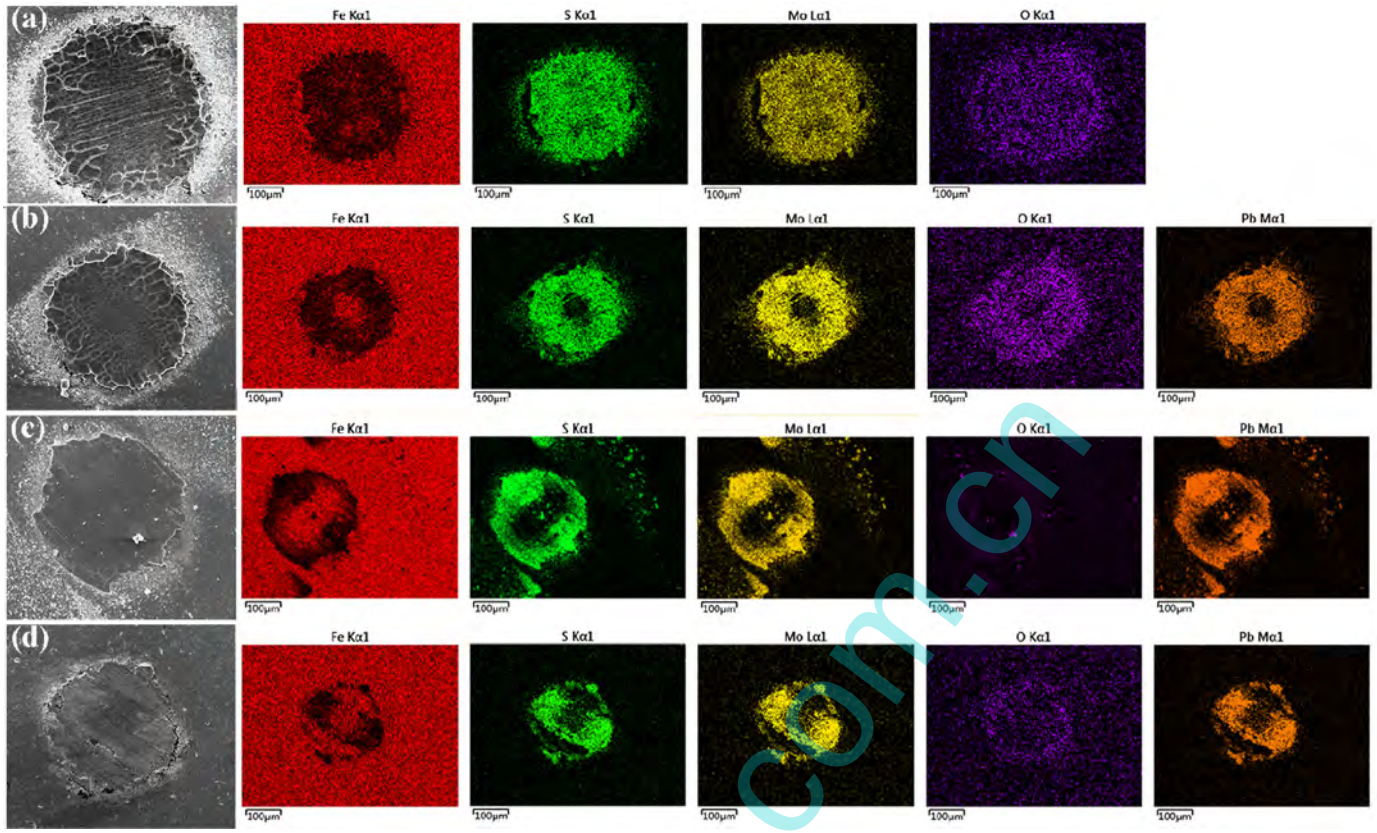

Fig. 8. Secondary electron images of the wear scars of a worn MoS_2, and MoS_2/Pb composite coatings with Pb content of (b) 2.3, (c) 6.8 and (d) 14.8 at% after sliding 10,000 cycles under 75% RH condition.

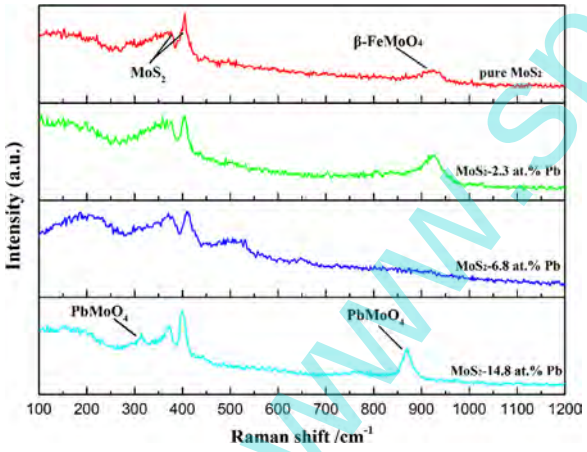

Fig. 9. Raman spectra of the wear scars of pure MoS_2 and MoS_2/Pb composite coatings after sliding 10,000 cycles under 75% RH condition.

To further evaluate the effect of the Pb content on the tribological performance of MoS_2/Pb composite coatings in humid air, the morphologies and the corresponding secondary electron images of the wear scars were examined after sliding friction of 10,000 cycles in 75% RH atmosphere. SEM micrograph in Fig. 8 reveals that for pure MoS_2 and MoS_2-2.3 at% Pb composite coatings, the transfer film appears many cracks along their boundary. For the pure MoS_2 coating, the transfer film in the contact zone appears to be uniform, while for the Pb doped coatings, very few transfer film is found in the center of contact surface. The same report was found in WS_2/Ag composite coatings against steel ball [51]. The transfer films of MoS_2/Pb composite coatings compose mainly of S, Mo and Pb, which is similar to MoS_2/Sb_2O_3/Au composite coating, where the transfer film consisted of Au and (0 0 2)-oriented crystalline MoS_2 [52]. The remarkable signal of oxygen was detected in the secondary images, which suggests that there is appreciable oxygen present in the transfer films of pure MoS_2, MoS_2-2.3 at% Pb and MoS_2-14.8 at% Pb composite coatings. While the signal of oxygen is hardly observed for MoS_2-6.8 at% Pb composite coating, which confirms that the coating with 6.8 at% Pb shows excellent antioxidant property. The wear scars were further investigated by Raman scattering to figure out the composition of the transfer films, as shown in Fig. 9. Features around 383 cm^{-1} and 408 cm^{-1} are consistent with the in-plane E_{2g} and out-of-plane A_{1g} vibrations of MoS_2, which are observed for all the four coatings. The peak around 926 cm^{-1} observed for pure MoS_2 and MoS_2-2.3 at% Pb composite coatings is assigned to β-$FeMoO_4$ [53,54]. For MoS_2-14.8 at% Pb composite coating, two characteristic peaks centered at 313 and 869 cm^{-1} are found to be correspond to $PbMoO_4$; however, no other Mo or Pb oxide is detected in the wear scar [20,55,56]. Furthermore, no evidence for Mo or Pb oxidation product (MoO_2, MoO_3, $FeMoO_4$ or $PbMoO_4$) is found for MoS_2-6.8 at% Pb composite coating, which is consistent with the results of secondary electron image. The shoulder peaks around 526 cm^{-1} (E_{1g}+LA(M)) and 650 cm^{-1} (A_{1g}+LA(M)) correspond to second-order MoS_2 vibrations [57–59]. The Raman results suggest that the pure MoS_2 and MoS_2/Pb composite coatings with low Pb content are easily oxidized into $FeMoO_4$ under humid environment, while the MoS_2/Pb composite coatings with high Pb content are oxidized into $PbMoO_4$. However, both $FeMoO_4$ and $PbMoO_4$ show poor tribological performance under room temperature, which accelerate the wear of

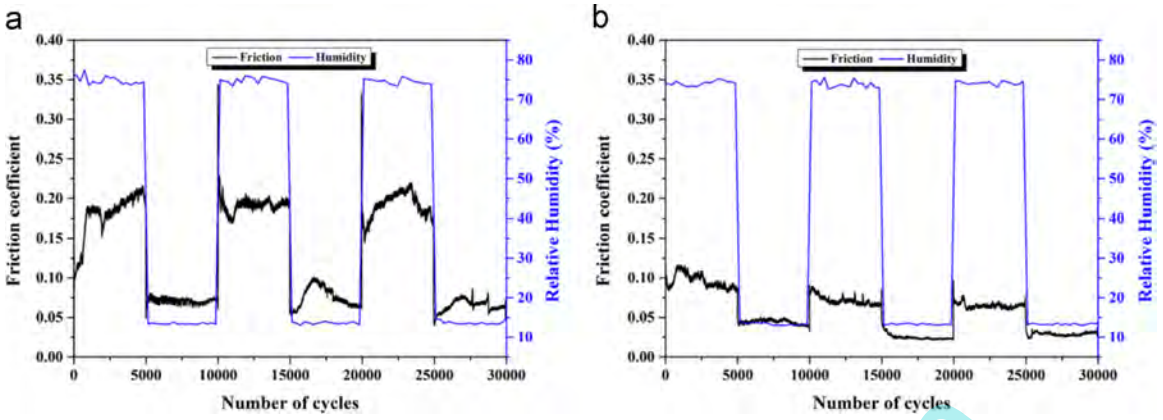

Fig. 10. Friction coefficient variation of (a) pure MoS_2 and (b) MoS_2-6.8 at% Pb composite coatings in tests for the environment varied from humid air (75% RH) to dry air (13% RH) every 5000 cycles.

MoS_2 coating [60,61]. Thus, the MoS_2/Pb coatings with relatively lower and higher Pb content show poor triboligical performance.

It is obvious that the tribological performance of pure MoS_2 coating under humid air can be significantly improved by the incorporation of Pb dopant, and the MoS_2-6.8 at% Pb composite coating shows the highest antioxidant property. Furthermore, it is believed that the coating shows high environmental adaptability owing to its high antioxidant property. Fig. 10 shows the variation of the friction coefficient under the environment varied between dry air (13 ± 1.5% RH) and humid air (75 ± 2.5% RH) every 5000 sliding cycles for both pure MoS_2 and the MoS_2-6.8 at% Pb composite coating. In humid cycles, the friction coefficients of pure MoS_2 coating are about 0.2, while the friction coefficients of the MoS_2-6.8 at% Pb composite coating are around 0.065–0.095. In dry cycles, pure MoS_2 coating exhibits an erratic friction coefficient of approximately 0.075, while the MoS_2-6.8 at% Pb composite coating shows a steady-state friction coefficient lower than 0.05. This suggests that the friction coefficient of MoS_2-6.8 at% Pb composite coating in dry cycles is less influenced by the former tribotest in humid cycles, and the coating shows higher environmental adaptability than pure MoS_2 coating.

4. Conclusions

The structure and mechanical behavior of the MoS_2 and MoS_2/Pb composite coatings were investigated. Furthermore, the friction and wear behavior of the coatings was evaluated under different humidity environments. The resulting wear scars were investigated in order to gain an understanding of friction mechanisms. The following conclusions are reached:

1. The composition of the MoS_2/Pb composite coatings can be controlled by changing the Pb target current during the deposition process. Both the hardness and elastic modulus increase at first and then decrease with the increasing of Pb concentration.
2. Under dry air (RH ≈ 13%), the antioxidant property of the composite coatings is negligible, while the mechanical property determines the wear properties. The antioxidant property of the MoS_2/Pb composite coatings becomes prominent as humidity increases. While in high humidity level (RH ≈ 75%), antioxidant property of the coating contributes to the tribological performance of the MoS_2/Pb composite coatings.
3. The performance of the controlling friction coefficient can be repeatedly and reversibly switched, permitting good performance during humidity environmental cycling as high antioxidant property.

Acknowledgments

The work was supported by the National Natural Science Foundation of China (Grants 51322508 and 51305433).

References

[1] C. Donnet, A. Erdemir, Solid lubricant coatings: recent developments and future trends, Tribol. Lett. 17 (2004) 389–397.
[2] T. Spalvins, Lubrication with sputtered MoS_2 films: principles, operation, and limitations, J. Mater. Eng. Perform. 1 (1992) 347–351.
[3] J. Grosseau-Poussard, P. Moine, M. Brendle, Shear strength measurements of parallel MoS_x thin films, Thin Solid Films 307 (1997) 163–168.
[4] P.D. Fleischauer, Fundamental aspects of the electronic structure, materials properties and lubrication performance of sputtered MoS_2 films, Thin Solid Films 154 (1987) 309–322.
[5] S. Prasad, J. Zabinski, N. McDevitt, Friction behavior of pulsed laser deposited tungsten disulfide films, Tribol. Trans. 38 (1995) 57–62.
[6] X. Zhang, R. Vitchev, W. Lauwerens, L. Stals, J. He, J.-P. Celis, Effect of crystallographic orientation on fretting wear behaviour of MoS_x coatings in dry and humid air, Thin Solid Films 396 (2001) 69–77.
[7] M.N. Gardos, The synergistic effects of graphite on the friction and wear of MoS_2 films in air, Tribol. Trans. 31 (1988) 214–227.
[8] M. Chhowalla, G.A. Amaratunga, Thin films of fullerene-like MoS_2 nanoparticles with ultra-low friction and wear, Nature 407 (2000) 164–167.
[9] T. Spalvins, Frictional and morphological properties of Au–MoS_2 films sputtered from a compact target, Thin Solid Films 118 (1984) 375–384.
[10] J.R. Lince, Tribology of co-sputtered nanocomposite Au/MoS_2 solid lubricant films over a wide contact stress range, Tribol. Lett. 17 (2004) 419–428.
[11] S.M. Aouadi, Y. Paudel, B. Luster, S. Stadler, P. Kohli, C. Muratore, C. Hager, A.A. Voevodin, Adaptive Mo_2N/MoS_2/Ag tribological nanocomposite coatings for aerospace applications, Tribol. Lett. 29 (2008) 95–103.
[12] J. Nainaparampil, A. Phani, J.E. Krzanowski, J. Zabinski, Pulsed laser-ablated MoS_2–Al films: friction and wear in humid conditions, Surf. Coat. Technol. 187 (2004) 326–335.
[13] J. Zabinski, M. Donley, S. Walck, T. Schneider, N. McDevitt, The effects of dopants on the chemistry and tribology of sputter-deposited MoS_2 films, Tribol. Trans. 38 (1995) 894–904.
[14] N. Renevier, V. Fox, D. Teer, J. Hampshire, Coating characteristics and tribological properties of sputter-deposited MoS_2/metal composite coatings deposited by closed field unbalanced magnetron sputter ion plating, Surf. Coat. Technol. 127 (2000) 24–37.
[15] I. Efeoglu, Ö. Baran, F. Yetim, S. Altıntaş, Tribological characteristics of MoS_2–Nb solid lubricant film in different tribo-test conditions, Surf. Coat. Technol. 203 (2008) 766–770.
[16] K. Wahl, D. Dunn, I. Singer, Wear behavior of Pb–Mo–S solid lubricating coatings, Wear 230 (1999) 175–183.
[17] J. Pimentel, T. Polcar, A. Cavaleiro, Structural, mechanical and tribological properties of Mo–S–C solid lubricant coating, Surf. Coat. Technol. 205 (2011) 3274–3279.
[18] A. Nossa, A. Cavaleiro, The influence of the addition of C and N on the wear behaviour of W–S–C/N coatings, Surf. Coat. Technol. 142 (2001) 984–991.
[19] J.R. Lince, $MoS_{2-x}O_x$ solid solutions in thin films produced by rf-sputter-deposition, J. Mater. Res. 5 (1990) 218–222.
[20] J. Zabinski, M. Donley, N. McDevitt, Mechanistic study of the synergism between Sb_2O_3 and MoS_2 lubricant systems using Raman spectroscopy, Wear 165 (1993) 103–108.

[21] J. Zabinski, M. Donley, V. Dyhouse, N. McDevitt, Chemical and tribological characterization of PbO–MoS_2 films grown by pulsed laser deposition, Thin Solid Films 214 (1992) 156–163.
[22] D. Kraut, G. Weise, W. Olbrich, G. Kampschulte, Low friction composite coating of Cr_xSi_y/MoS_2 on steel, Surf. Coat. Technol. 60 (1993) 515–520.
[23] H. Nyberg, J. Sundberg, E. Särhammar, F. Gustavsson, T. Kubart, T. Nyberg, U. Jansson, S. Jacobson, Extreme friction reductions during initial running-in of W–S–C–Ti low-friction coatings, Wear 302 (2013) 987–997.
[24] D. Teer, New solid lubricant coatings, Wear 251 (2001) 1068–1074.
[25] L. Isaeva, J. Sundberg, S. Mukherjee, C.J. Pelliccione, A. Lindblad, C.U. Segre, U. Jansson, D. Sarma, O. Eriksson, K. Kádas, Amorphous W–S–N thin films: the atomic structure behind ultra-low friction, Acta Mater. 82 (2015) 84–93.
[26] F. Gustavsson, S. Jacobson, A. Cavaleiro, T. Polcar, Ultra-low friction W–S–N solid lubricant coating, Surf. Coat. Technol. 232 (2013) 541–548.
[27] A. Voevodin, J. Zabinski, Supertough wear-resistant coatings with 'chameleon' surface adaptation, Thin Solid Films 370 (2000) 223–231.
[28] J. Zabinski, J. Bultman, J. Sanders, J. Hu, Multi-environmental lubrication performance and lubrication mechanism of MoS_2/Sb_2O_3/C composite films, Tribol. Lett. 23 (2006) 155–163.
[29] B. Vierneusel, T. Schneider, S. Tremmel, S. Wartzack, T. Gradt, Humidity resistant MoS_2 coatings deposited by unbalanced magnetron sputtering, Surf. Coat. Technol. 235 (2013) 97–107.
[30] T.W. Scharf, S.V. Prasad, Solid lubricants: a review, J. Mater. Sci. 48 (2013) 511–531.
[31] K.F. Koo, G.L. Schrader, Method for preparing basal oriented molybdenum disulfide (MoS2) thin films, US Patent 5370778, Dec., 1994.
[32] K.J. Wahl, D.N. Dunn, I.L. Singer, Wear behavior of Pb–Mo–S solid lubricating coatings, Wear 230 (1999) 175–183.
[33] J. Moser, F. Lévy, Random stacking in MoS_{2-x} sputtered thin films, Thin Solid Films 240 (1994) 56–59.
[34] W.Y. Lee, K.L. More, Crystal orientation and near-interface structure of chemically vapor deposited MoS_2 films, J. Mater. Res. 10 (1995) 49–53.
[35] P.D. Fleischauer, Effects of crystallite orientation on environmental stability and lubrication properties of sputtered MoS_2 thin films, ASLE Trans. 27 (1984) 82–88.
[36] J. Dupin, D. Gonbeau, I. Martin-Litas, P. Vinatier, A. Levasseur, Amorphous oxysulfide thin films MO_yS_z (M=W, Mo, Ti) XPS characterization: structural and electronic pecularities, Appl. Surf. Sci. 173 (2001) 140–150.
[37] J. Yu, C.Y. Jimmy, B. Cheng, X. Zhao, Photocatalytic activity and characterization of the sol-gel derived Pb-doped TiO_2 thin films, J. Sol-Gel Sci. Technol. 24 (2002) 39–48.
[38] R. Reiche, R. Thielsch, S. Oswald, K. Wetzig, XPS studies and factor analysis of PbS nanocrystal-doped SiO_2 thin films, J. Electron. Spectrosc. Relat. Phenom. 104 (1999) 161–171.
[39] S. Chen, W. Liu, L. Yu, Preparation of DDP-coated PbS nanoparticles and investigation of the antiwear ability of the prepared nanoparticles as additive in liquid paraffin, Wear 218 (1998) 153–158.
[40] G. Strapasson, P. Badin, G. Soares, G. Machado, C. Figueroa, R. Hubler, A. Gasparin, I. Baumvol, C. Aguzzoli, E. Tentardini, Structure, composition, and mechanical characterization of dc sputtered TiN-MoS_2 nanocomposite thin films, Surf. Coat. Technol. 205 (2011) 3810–3815.
[41] I. Bertóti, M. Mohai, N. Renevier, E. Szilágyi, XPS investigation of ion beam treated MoS_2–Ti composite coatings, Surf. Coat. Technol. 125 (2000) 173–178.
[42] A. Boronin, V. Bukhityarov, A. Vishnevskii, G. Boreskov, V. Savchenko, XPS and UPS studies of oxygen adsorption over clean and carbon-modified silver surfaces, Surf. Sci. 201 (1988) 195–210.
[43] A.V. Naumkin, A. Kraut-Vass, C.J. Powell, NIST X-ray photoelectron spectroscopy database. Measurement Services Division of the National Institute of Standards and Technology (NIST) Technology Services, 2008.
[44] X.Z. Ding, X.T. Zeng, X.Y. He, Z. Chen, Tribological properties of Cr-and Ti-doped MoS_2 composite coatings under different humidity atmosphere, Surf. Coat. Technol. 205 (2010) 224–231.
[45] H.S. Myung, H.M. Lee, L.R. Shaginyan, J.G. Han, Microstructure and mechanical properties of Cu doped TiN superhard nanocomposite coatings, Surf. Coat. Technol. 163 (2003) 591–596.
[46] J.G. Han, H.S. Myung, H.M. Lee, L.R. Shaginyan, Microstructure and mechanical properties of Ti–Ag–N and Ti–Cr–N superhard nanostructured coatings, Surf. Coat. Technol. 174 (2003) 738–743.
[47] W. Gulbiński, T. Suszko, Thin films of Mo_2N/Ag nanocomposite—the structure, mechanical and tribological properties, Surf. Coat. Technol. 201 (2006) 1469–1476.
[48] J.L. He, Y. Setsuhara, I. Shimizu, S. Miyake, Structure refinement and hardness enhancement of titanium nitride films by addition of copper, Surf. Coat. Technol. 137 (2001) 38–42.
[49] A. Leyland, A. Matthews, On the significance of the H/E ratio in wear control: a nanocomposite coating approach to optimised tribological behaviour, Wear 246 (2000) 1–11.
[50] M. Simmonds, A. Savan, E. Pflüger, H. Van Swygenhoven, Mechanical and tribological performance of MoS_2 co-sputtered composites, Surf. Coat. Technol. 126 (2000) 15–24.
[51] S. Xu, X. Gao, M. Hu, J. Sun, D. Wang, F. Zhou, L. Weng, W. Liu, Morphology evolution of Ag alloyed WS_2 films and the significantly enhanced mechanical and tribological properties, Surf. Coat. Technol. 238 (2014) 197–206.
[52] T.W. Scharf, P.G. Kotula, S.V. Prasad, Friction and wear mechanisms in MoS_2/Sb_2O_3/Au nanocomposite coatings, Acta Mater. 58 (2010) 4100–4109.
[53] Y. Wang, P. He, W. Lei, F. Dong, T. Zhang, Novel $FeMoO_4$/graphene composites based electrode materials for supercapacitors, Compos. Sci. Technol. 103 (2014) 16–21.
[54] N. Boucherit, H.L. Goff, S. Joiret, Raman studies of corrosion films grown on Fe and Fe-6Mo in pitting conditions, Corros. Sci. 32 (1991) 497–507.
[55] M.R.D. Bomio, L.S. Cavalcante, M.A.P. Almeida, R.L. Tranquilin, N.C. Batista, P.S. Pizani, M.S. Li, J. Andres, E. Longo, Structural refinement, growth mechanism, infrared/Raman spectroscopies and photoluminescence properties of $PbMoO_4$ crystals, Polyhedron 50 (2013) 532–545.
[56] N.T. Vitt, M.S. Donley, J.S. Zabinski, Utilization of Raman spectroscopy in tribochemistry studies, Wear 166 (1993) 65–72.
[57] H. Singh, K.C. Mutyala, R.D. Evans, G.L. Doll, An investigation of material and tribological properties of Sb_2O_3/Au-doped MoS_2 solid lubricant films under sliding and rolling contact in different environments, Surf. Coat. Technol. 284 (2015) 281–289.
[58] B. Chakraborty, H.S.S. Matte, A.K. Sood, C.N.R. Rao, Layer-dependent resonant Raman scattering of a few layer MoS_2, J. Raman. Spectrosc. 44 (2013) 92–96.
[59] G.L. Frey, R. Tenne, M.J. Matthews, M.S. Dresselhaus, G. Dresselhaus, Raman and resonance Raman investigation of MoS_2 nanoparticles, Phys. Rev. B 60 (1999) 2883.
[60] J.S. Zabinski, A.E. Day, M.S. Donley, C. Dellacorte, N.T. McDevitt, Synthesis and characterization of a high-temperature oxide lubricant, J. Mater. Sci. 29 (1994) 5875–5879.
[61] S. Fayeulle, P.D. Ehni, Paper V (ii) role of transfer films in wear of MoS_2 coatings, Tribol. Ser. 17 (1990) 129–138.